

## CHAPTER – 4

# LATE QUATERNARY SEDIMENTS ALONG KATROL HILL FAULT ZONE

The Quaternary sediments in the Kachchh region can be observed as clay deposits occupying the Ranns, the alluvial plains occupying the Banni, which further southwards merge with the colluvial fans, pedogenized fluvial sand-silt and gravels, assorted colluvial deposits and miliolites are found occupying the fault scarp bases and cliff sections of various streams (Maurya et al., 2003c). Sporadic occurrences of Quaternary sediments in the Katrol Hill Range (KHR) comprise of boulder colluvium at the base, overlain successively by aeolian miliolite, valley-fill/ fluvial miliolite (reworked), sandy alluvium and scarp derived colluvium (Patidar et al., 2007). Figure 4.1 shows a generalised lithostratigraphy of all the varieties of Quaternary deposits found in the Katrol Hill Range along with the Mesozoic rocks present at the basement. The thickness of each unit comprising the litholog is relative and varies from location to location.

The bouldery colluvium deposits found overlying the Mesozoic rocks at the basement (Figure 4.1) are degraded debris derived from the scarps and are poorly sorted comprising angular to sub-rounded boulders, cobbles, pebbles and fine sand, derived from the formations consisting of shales, sandstones and siltstones. The overlying aeolian and valley-fill or fluvially reworked miliolites are the most commonly encountered varieties of miliolites.

Miliolite deposits of both aeolian and fluvial origins are the most commonly found in the KHR across diverse geomorphic settings such as hill slopes, valleys and depressions, wind gaps and ravines. Topographic profiles are constructed as shown in Figure 4.2b, which pass across the KHR and KHF and show the occurrence of these deposits. The transects of the topographic profiles are drawn in Figure 4.2a. The miliolite deposits reported from the Kachchh and Kathiawar regions form a distinct stratigraphic unit belonging to Middle to Late Pleistocene age. Carter (1849) identified these deposits as '*miliolitic limestone*', as they are essentially bioclastic carbonate deposits. Biswas (1971) for the first time described the distribution of these deposits in the field and their depositional environment. These deposits are mainly observed in the Great Rann of Kachchh, the Banni plains, Northern Hill Range and the coastal alluvial plains (Thakkar et al., 1999; Maurya et al., 2003a). The miliolite deposits mark an important horizon that acts a chronograph and deliver information, which

helps decipher various geological processes regulated by the change in climate and tectonics (Biswas, 1971; Thakkar et al., 1999).

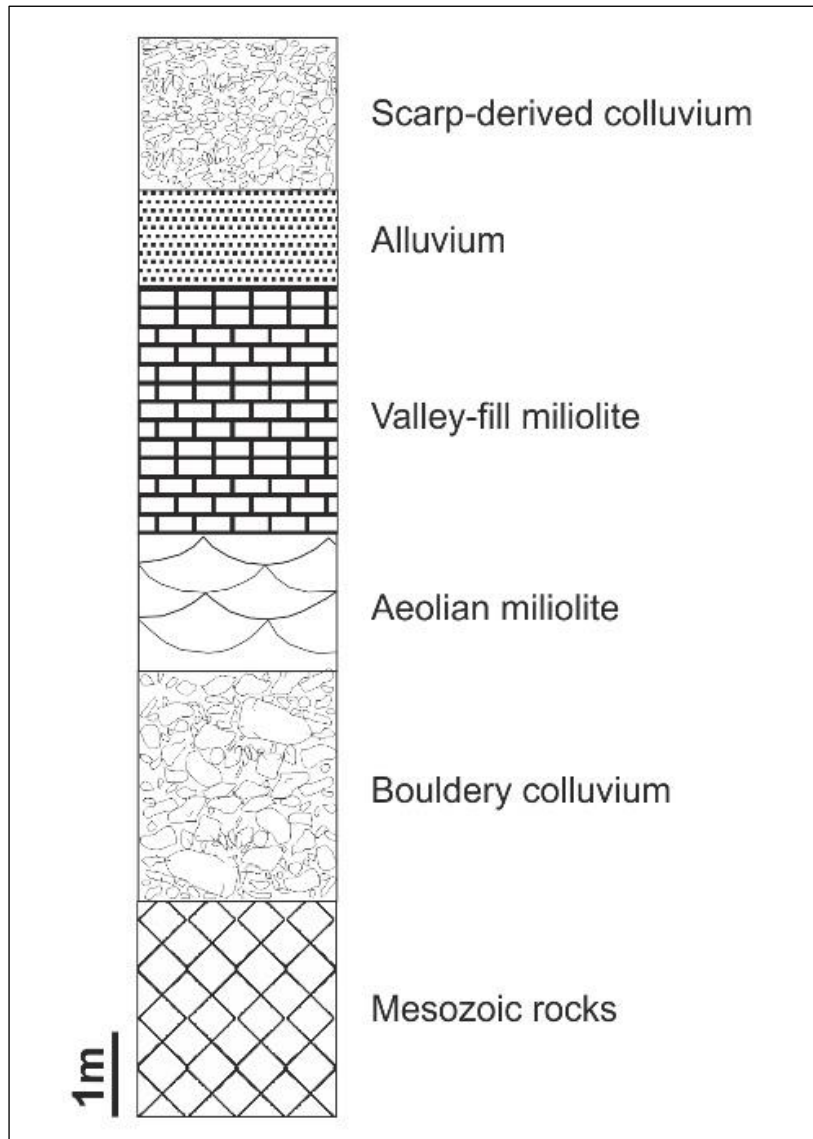


**Figure 4.1** Generalised composite lithostratigraphy of exposed Quaternary sediments along the Katrol Hill Fault zone. Modified from Patidar (2010).

Patel and Allahabadi (1988) classified the deposits that occur on the southern slopes as windward deposits and those on northern slopes as leeward deposits (Figure 4.3a). The aeolian miliolite is also observed as obstacle dunes occupying the slope of the hills and depressions, where there is a sharp change in the wind velocity (Figure 4.3b). Thicker and more pronounced sedimentation of aeolian miliolites is observed on the southern slopes of the Katroll Hill Range (Talati and Bhatt, 2018b). These deposits are characterized by medium to fine grained sediments and moderate to well sorted carbonate sand grains. The field characteristics include large scale aeolian cross beddings (Figure 4.3c).

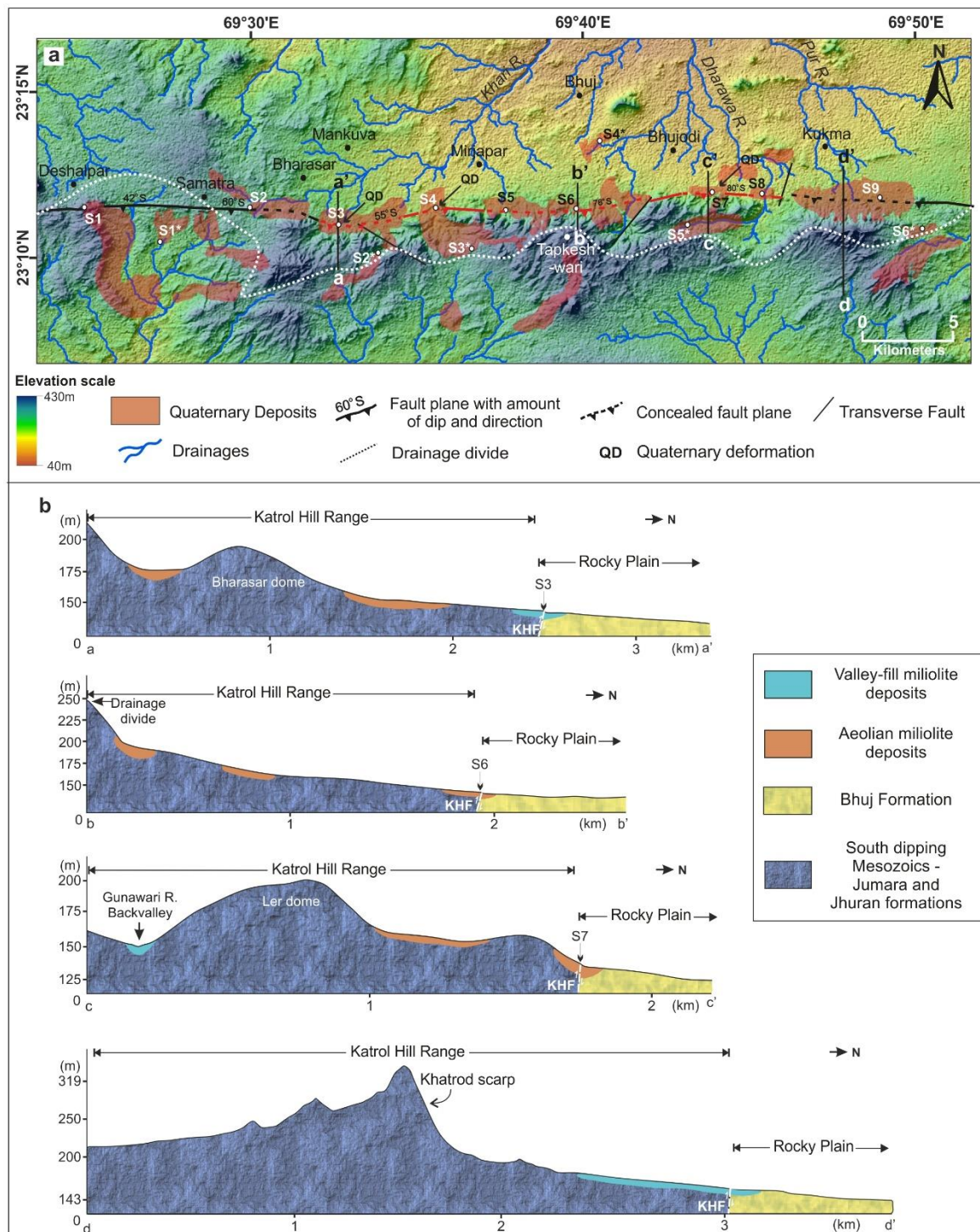


**Figure 4.2 a.** Geological map/DEM of the study area showing KHF and mapped Quaternary sediments. Red colored fault line shows active trace of the KHF based on present study. Note the sporadic nature of Quaternary sediment cover. S1-S9 and S1\*-S6\* mark the sampling location for microscopic studies. **b.** Representational N-S trending topographic profiles across the KHF zone showing the occurrences and stratigraphic set-up of Quaternary deposits in Katrol Hill Range (KHR) at Bharasar (a-a'), Tapkeshwari (b-b') and Bhujodi (c-c') and north of the Khatrol scarp (d-d'). Few sampling locations falling on the topographic profiles are also marked.

On the other hand, the valley-fill miliolite of fluvial origin occupies the steep vertical scarps and banks of various rivers (Figure 4.4a, b) giving a well-developed sheet like geometry. These deposits are seen at physiographically lower heights and along the river cliffs, which have experienced incision. These deposits contain fine grained and moderately sorted sediments. They do not display any noticeable sedimentary structures in the field. Finally, the fluvially reworked miliolites also belong to the fluvial origin as evidenced by well-stratified sandy sheet comprising of pebbles and gravels (Figure 4.5a, b). These deposits display fluvial sedimentary structures such as small scour and fill, cross beddings with small and large clasts belonging to Mesozoic rocks.

The fluvio-aeolian miliolite deposits are overlain by fine grained alluvial deposits (Figure 4.4b), which are occasionally observed in the cliff-sections of the north flowing rivers of the KHR. The areas comprising of these deposits towards the north of the scarps are widely utilized as agricultural lands.



**Figure 4.3** a. Aeolian miliolite exposure found towards the north of Bharasar dome. Height of marker is 5.5ft. b. Aeolian miliolite deposits covering the foot-hill region north of the scarp found ~3 km south of Bhuj town. c. Close view of distinct aeolian cross-bedding displayed by a miliolite outcrop found south of Bharasar. Length of marker is 7 inches.

According to the chronologic data presented by Patidar et al. (2007; 2008), the fluvial miliolites along with the alluviums deposited in the post-miliolite phase of fluvial deposition during the Late Pleistocene phase of aggradation. The alluvial deposits, while at some places the fluvial miliolite deposits are overlain by the scarp-derived colluvium, which is the youngest Quaternary deposit among all others described till now (Patidar et al., 2007). These deposits consist of the scarp-derived clasts of older Mesozoic rocks and show presence of carbonates, which are obtained from the previously deposited miliolite sediments. They display different degrees of compaction ranging from semi-consolidated to unconsolidated.

Deposition of the miliolites in Kachchh took place episodically. The pre-miliolitic phase of deposition occurred during the early Quaternary times and the post-miliolitic phase commenced in the Late Pleistocene and continued to the present. The Quaternary tectonic activity can be decoded from the depositional phases of miliolites (Thakkar et al., 1999).

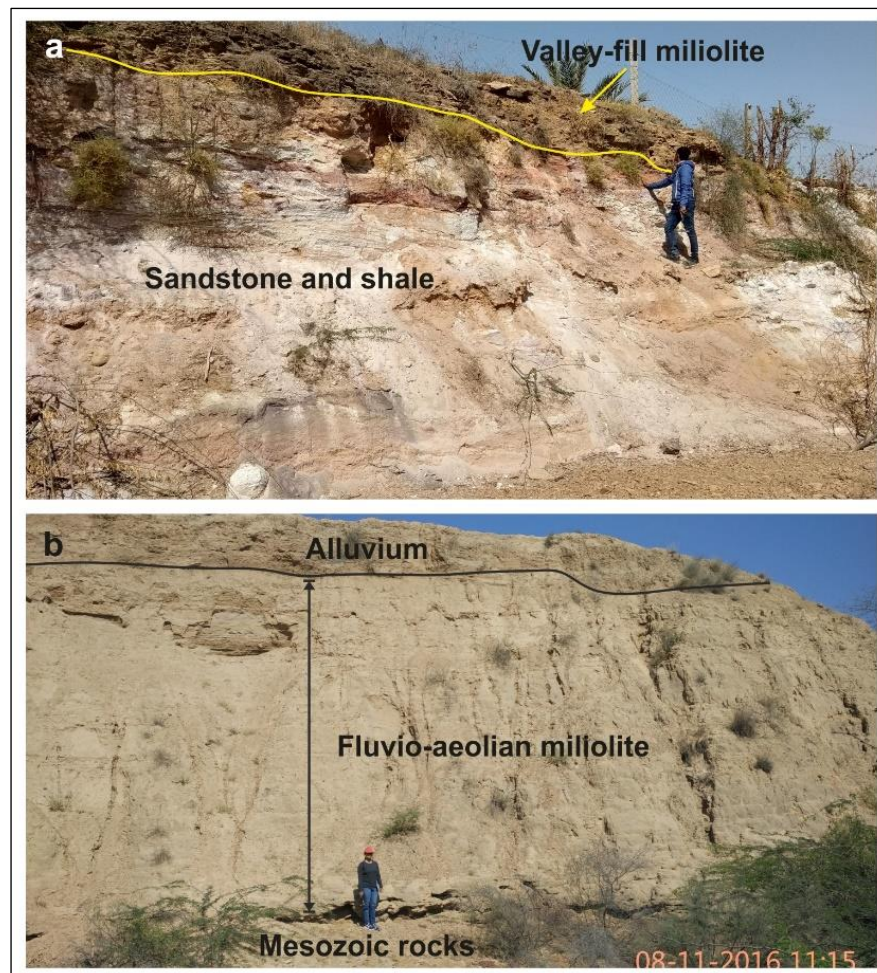


**Figure 4.4** a. Thin and eroded layer of valley-fill miliolite deposited as sheet miliolites over sandstone and shale sequences of Jumara Formation (older Mesozoic rocks) in the cliff section of a stream located north of Tapkeshwari road. b. Incised cliff section of the Gunawari river showing fluvio-aeolian miliolite deposits overlying the Mesozoic rocks. Note the variation in thickness of the valley-fill miliolite deposits. Height of markers in both a, b is 5.5ft.

Available  $^{230}\text{Th}/^{234}\text{U}$  chronological data show that the aeolian miliolite deposition in KHF zone spanned the Late Pleistocene up to ~42 ka B.P. (Baskaran, 1989a). Bhattacharya et al. (2013; 2014) used the Optically Simulated Luminescence (OSL) dating method and reported the ages of fluvial gravel and sand units associated with miliolitic sand to be in the range from 11.8 – 7.1 ka B.P.



**Figure 4.5** a. Close view of distinct horizontal sheets observed in valley-fill miliolite deposits found in the cliff section of Gunawari reservoir towards the west of Ler area. b. Close view of fluvially reworked miliolites showing horizontal planar bedding and consisting of cobble sized clast. Length of marker in both a, b is 1.5ft.

## **PETROGRAPHIC CHARACTERISTICS OF MILIOLITE DEPOSITS**

The miliolite deposits found in the Kachchh basin typically portray the characteristics of pelletoidal calcareous sandstones. Commonly, the miliolite rocks are white to light brownish in colour and turn grey on weathering (Biswas, 1971). Sand, calcareous pellets and cement form the three essential components of all the three different kinds of miliolite deposits in varying proportions with occasional presence of ooliths and little amount of clay in the matrix. These rocks rarely consist of few feldspar grains and typically lack heavy minerals (Biswas, 1971). According to the classification of Folk (1959), these rocks are classified as coarse calcarenite in texture and display very high degree of sorting as indicated by uniformity in shape and grain size (Biswas, 1971). The majority of the miliolite grains range in size from 0.9 phi to 2.5 phi, finely skewed and display platykurtic to mesokurtic distribution (Talati and Bhatt, 2018b). This rock is poorly cemented due to little amount of cement holding the sand grains and pellets together. The cement is mainly microcalcitic and sometimes ferruginous (hematitic or limonitic) (Biswas, 1971). Commonly, these rocks comprise of sand and pellets and lack the cementing material, which gives rise to the friable nature of these rocks; while, the varieties with more calcareous constituents are more compact and well bedded. The sand consists of clear quartz and displays medium to fine grained, clastic nature and comprises of ~60% – 90% of the bulk composition of the rock. Very high degree of roundness (~0.9) and sphericity is displayed by the quartz grains constituting the rock. Approximately 40% of the rock comprises of the spheroidal to ellipsoidal pellets, which comprise of microcrystalline calcite. Sometimes, faecal pellets may be present; while worn-out foraminiferal tests are consistently present in every sample of miliolite rocks. Far-off distance transportation is indicated by rolled and abraded foraminiferal tests. Quite indistinguishable from the pellets are rolled and tiny shells of gastropods and lamellibranchs are also frequently present.

Different and rare rock types such as arenaceous pelmicrite or arenaceous oomicrite, pelletic oomicrite and arenaceous oolitic pelmicrite are encountered from various localities such as northern slope of Dhinodhar Hill, Jhurio Hill and Dhruviya Hill respectively (Biswas, 1971). The above-mentioned rock types are formed as a consequence of increase in the pellet percentage and reduction in the clastic sand content in the common miliolite rock assemblage.

Varying percentages of detrital content such as 41%, 55% and 68% can be observed in the aeolian, valley-fill and fluvially reworked miliolites (Talati and Bhatt, 2018b). Hence, the valley-fill and fluvially reworked varieties comprise of comparatively higher amount of

locally derived detrital material and previously reworked carbonate grains. The diagenetic properties such as less compaction, moderate to high porosity, cement morphology and mineralogy point towards the diagenesis of miliolite rocks in the fresh water vadose environment with seasonally phreatic conditions as indicated by low magnesian microsparite cement and porosity modifications (Bhatt and Patel, 1996). The abrasion experiment performed on the miliolite deposits found in the Katrol Hill Range by Talati and Bhatt (2018b) shows that the erodibility of these deposits is very high as the erosion experiment results in ~30% loss in its weight after the experiment, which is almost twice to that of Mesozoic substrate rocks.

Thin sections of miliolite deposits of both aeolian and fluvial origin found in the study area were analysed to classify them on the basis of their mineral assemblage and textural characteristics. The samples collected from the sites S1, S2 and S9 (marked in Figure 4.2a) are used to prepare the thin-section, wherein, the site S1 belongs to aeolian origin of miliolite deposits while the remaining two sites S2 and S9 belong to that of fluvial origin. The miliolite samples belonging to both aeolian and fluvial origins collected from various outcrops located near the Katrol Hill Fault (KHF) zone display almost identical assemblage of different components, which comprise of mineral grains of quartz, pyroxene microcline and (augite – very rare) and, bioclasts of bryozoans, foraminifera, algae, shell fragments and pellets. These components are observed to be bound together by calcareous cementing material. The difference between the aeolian and fluvial varieties of miliolite rocks can be observed in terms of the roundness of the grains, grain sorting and the type of contact between the grains, which indicates compaction of the rock. The fluvial miliolite consists of sub-rounded to sub-angular grains, which are poorly sorted. The grain size varies from 0.2 - <1mm.

It can be observed in Figure 4.6a that the amount of calcareous foraminiferal tests is less and occurrence of quartz grains is more as compared to that of aeolian miliolites. In Figure 4.6b, the point contact relation between the grains is observed. These deposits have experienced very less compaction after its deposition as indicated by the point contact relation between the grains. The amount of broken shell fragments is comparatively more, which indicates the fluvially reworked nature of these miliolite deposits. The presence of microcline (alkali) feldspar in Figure 4.6b indicates that the rock has undergone weak diagenetic changes. Occasionally, foraminiferal tests like the one observed in Figure 4.6c can be observed in the fluvially reworked miliolite samples.

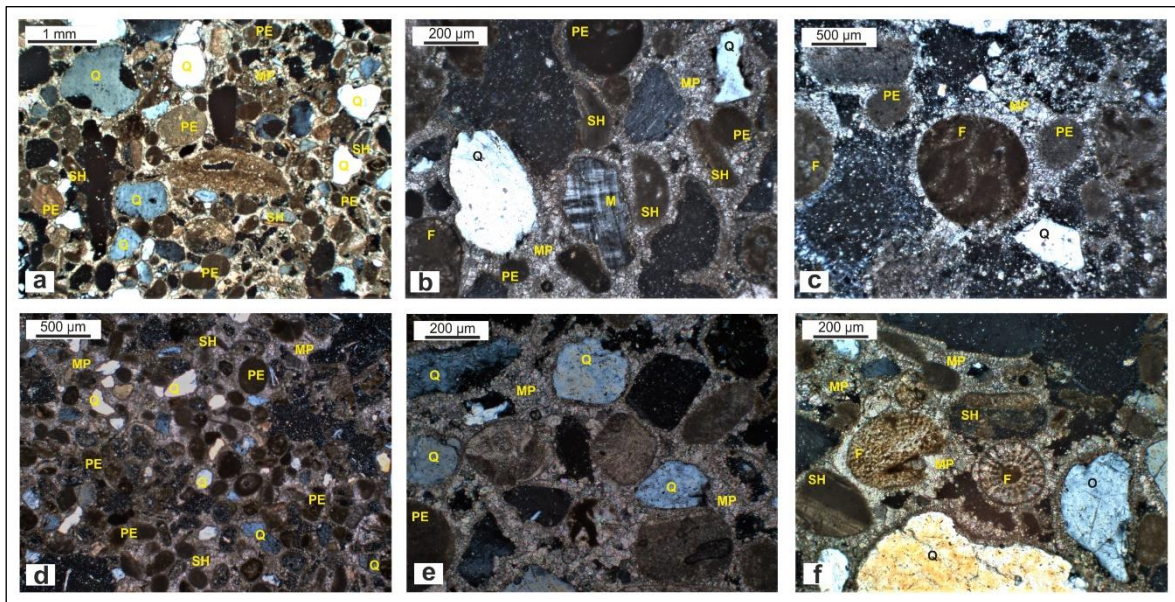


**Figure 4.6** Thin-section photomicrographs of fluviually reworked (a to c) and aeolian miliolite deposits (d to f) sampled away from the KHF zone. **a.** (4x-XPL) Poorly sorted and sub-rounded to sub-angular detrital mineral grains are mostly quartz with calcareous foraminiferal tests. **b.** (10x-XPL) Point contact relation between the grains and recrystallization of calcitic cement forms micro-sparite between the inter-granular spaces. Rarely observed microcline pointing towards weak diagenetic activity. **c.** (10x-XPL) Occasional presence of an intact foraminiferal test. **d.** (2.5x-XPL) Well sorted and rounded to sub-rounded detrital quartz grains with peloid bioclasts and occasional shell fragments embedded in calcareous cement. **e.** (10x-XPL) Point contact relation between the grains and micro-sparite formation in the inter-granular spaces due to recrystallization of calcitic cement. **f.** (10x-XPL) Occasional presence of orthoclase feldspar indicating weak diagenetic activity. (D-Dissolution, MP-Micro-sparite, O- Orthoclase, P-Porosity, PE-Peloid, Q-Quartz, M-Microcline, SH-Shell fragments, F-Foraminiferal tests).

In contrast to the above characteristics of fluvial miliolites, the aeolian miliolite sample in Figure 4.6d show rounded to sub-rounded grains and are well sorted. The grain size is ~0.2 – 0.5mm (Figure 4.6d). In Figure 4.6e, it can be seen that the quartz grains and bioclasts rarely come in contact with each other and hence, display point contact relation. This point contact relation between the grains indicates very less or minimal compaction of the rock after its deposition, which in turn determines the porous nature of the rock. The presence of orthoclase (alkali) feldspar in Figure 4.6f demonstrates that the rock has undergone weak diagenetic activity. Micro-sparite precipitate can be seen rimmed around the bioclasts of both aeolian and fluvial miliolites (Figure 4.6c and f). All above evidences indicate the deposition under the freshwater-vadose environment (Bhatt and Patel, 1996).

## **SCANNING ELECTRON MICROSCOPY (SEM) OF QUARTZ GRAINS OF MILIOLITES**

The surfaces of quartz and various other mineral grains are characterized by microtextures, which are basically micrometre-sized imprints, when observed under a powerful microscope, for e.g., a scanning electron microscope (SEM). Most of the sedimentary environments contain quartz grains, which markedly preserve microtextures of multiple environments they have been in, due to its unique mineralogical properties (Mahaney, 2002). The study of these microtextures of quartz grains from different geological backgrounds has been recognized as a useful method that enables the reconstruction of past environments (Bull, 1961). Various authors such as Porter (1962), Krinsley and Donahue (1968), Whalley and Krinsley (1974), Mahaney and Kalm (2000), Mahaney et al. (2001), Mahaney (2002) and Vos et al. (2014) have effectively depicted an essential role of distinct processes responsible for the development of surface textures or microtextures on the quartz grains. Discussed next are the microtextures observed on the representative quartz grain surfaces, which characterise the fluviually reworked and aeolian miliolite samples – S3, S4, S6 and S8, and S5 and S7 respectively (marked in Figure 4.2a) found in the Katrol Hill Fault zone.

### **Fluvial microtextures**

The quartz grain surface and the grain boundaries show various breakage patterns (marked by arrows in Figure 4.7) which is the most common feature observed in most of the grains. One of the quartz grains (Figure 4.7a) shows highly fractured surface with unevenly broken edges and appears to have undergone solution action, as very less amount of silica is found precipitated over its rough and weathered surface.

Another grain shows unoriented fracturing of the surface (Figure 4.7b) with prominent radial fractures in the central portion of the surface. Here, the right facet of the grain shows smooth fracture which likely indicates a fresh fractured split grain surface. The breakage on some grain surfaces (Figure 4.7c, d) can be seen in the form of step-like fractures, which are approximately parallel to each other. Additionally, the conchoidal fracture planes of these grains (Figure 4.7c, d) also display deeply inscribed arcuate and straight fractures in the form of steps. The depths of the steps are usually larger than 2-3  $\mu\text{m}$ , with spacing of  $\sim 5 \mu\text{m}$  between successive steps. These fracture patterns mostly form during impacts or pressures when the conchoidal fracture plane intersects with the cleavage planes of the quartz crystal. Therefore, they are said to be genetically related to conchoidal fractures (Vos et al., 2014). Impressions of large breakage blocks (Figure 4.7d) can be observed on

the grain surface, giving the appearance of a fresh fractured surface, as it lacks any dissolution etching or precipitation features (Mahaney, 2002). Conchoidal fractures; a microtextural property typical of a quartz grain are often visible (Figure 4.7e, f). This is the most commonly occurring feature on the quartz grains recovered from most of the environments; characterized by curved, shell-like breakage patterns (Figure 4.7f) and a lack of pronounced cleavage directions (Vos et al., 2014). The fractures appear to be smoothed by solution action (Figure 4.7e).

Also, sawtooth shaped fracture pattern (Figure 4.7f) along with Si globules having precipitated over most of the grain surface is visible in the microphotograph. Some grains (Figure 4.7g to l) display pitted and grooved nature all over the surface with prominent fracture patterns and chemical etching. V-shaped percussion marks (Figure 4.7g) can be observed on the grain surface in the central and left portion, which are more or less triangular shaped depressions, with a maximum diameter of  $\sim < 5 \mu\text{m}$  and an average depth of  $\sim 0.1 \mu\text{m}$ . Such depressions usually become narrower as they reach deeper into the grain until they fade away completely (Margolis and Krinsley, 1974). Typically, the v-shaped cracks are randomly oriented, reflecting the randomly occurring collisions between grains (Margolis and Krinsley, 1974) and resulting from a group of plates along the cleavage surfaces being broken at a number of points (Krinsley and Doornkamp, 1973). The grain surface here (Figure 4.7g) also appears to be chemically altered. Furthermore, some grains (Figure 4.7h, i) show chemically altered and etched grain surface with crescentic gouges which result from severe grain-to-grain collisions (Campbell, 1963) or by the chiselling action of bladed fragments of other grains (Mahaney, 2002). They resemble the initial stage of a curved, small ( $< 50 \mu\text{m}$ ) conchoidal fracture, which was not able to develop into a complete fracture plane due to the lack of impact energy. Irregular pits and depressions on the grain surface (Figure 4.7j), may have resulted due to the solution action on the grain surface, which causes dissolution of inclusions. The occurrence and appearance of the solution pits depend on the amount of chemical activity and the dwell time in the environment aiding the dissolution of quartz. Therefore, it is often difficult to distinguish between remnants of mineral inclusions and solution pits (Higgs, 1979). Another grain (Figure 4.7k) shows elongated, linear and curved shallow depressions on the grain edge. It appears that solution and precipitation features have filled the depressions and dissolved the protruding areas on the surface to produce such features with rounded or blunt edges. The solution activity has smoothed the grain edge, which earlier exposed the cleavage plates that are faintly visible in the upper portion of the grain.

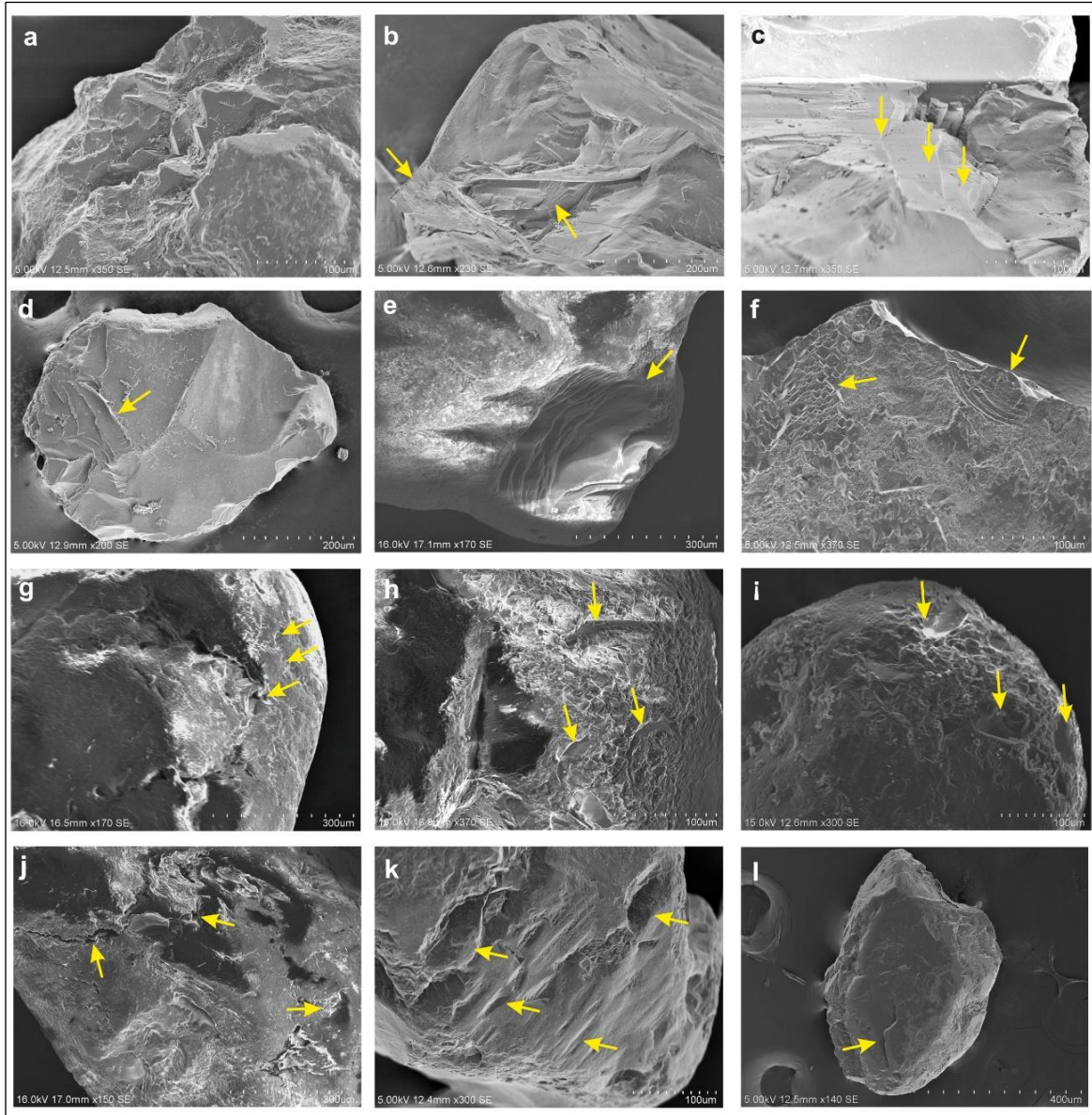


**Figure 4.7** SEM photomicrographs of representative quartz grains of fluvial miliolite samples from the KHF zone displaying breakage patterns. **a.** Highly fractured quartz grain surface with unevenly broken edges and undergone solution action and silica precipitation over its rough and weathered surface. **b.** Unoriented surface fracturing of grain with prominent radial fractures marked by arrows. **c.** Breakage in the form of step-like fractures, approximately parallel to each other. **d.** Deeply inscribed arcuate and straight fractures in the form of steps observable on the conchoidal fracture planes of the grains. **e.** Conchoidal fractures smoothed by solution action. **f.** Conchoidal fractures in shell-like breakage pattern (right side arrow) and sawtooth shaped fractures (left side arrow) with silica precipitation. **g.** chemically altered grain surface with v-shaped percussion marks. **h.** and **i.** Chemically altered and etched grain surface with crescentic gouges. **j.** Irregular pits and depressions on the grain surface. **k.** Solution action has filled the depressions and dissolved the protruding areas of the grain to produce elongated, linear and curved shallow depressions on the grain edge. **l.** Irregularly fractured surface with grooves and depressions with highly weathered grain edges.

Irregularly fractured surface with grooves and depressions (Figure 4.7i) is observed with highly weathered grain edges due to chemical action. The grain surfaces (Figure 4.7) also consist of upturned plates which are not uniformly present all over the surface but scarcely located at a few portions on the surface.

A uniform Si covering can be observed on an irregularly pitted and rough grain surface (Figure 4.8a).

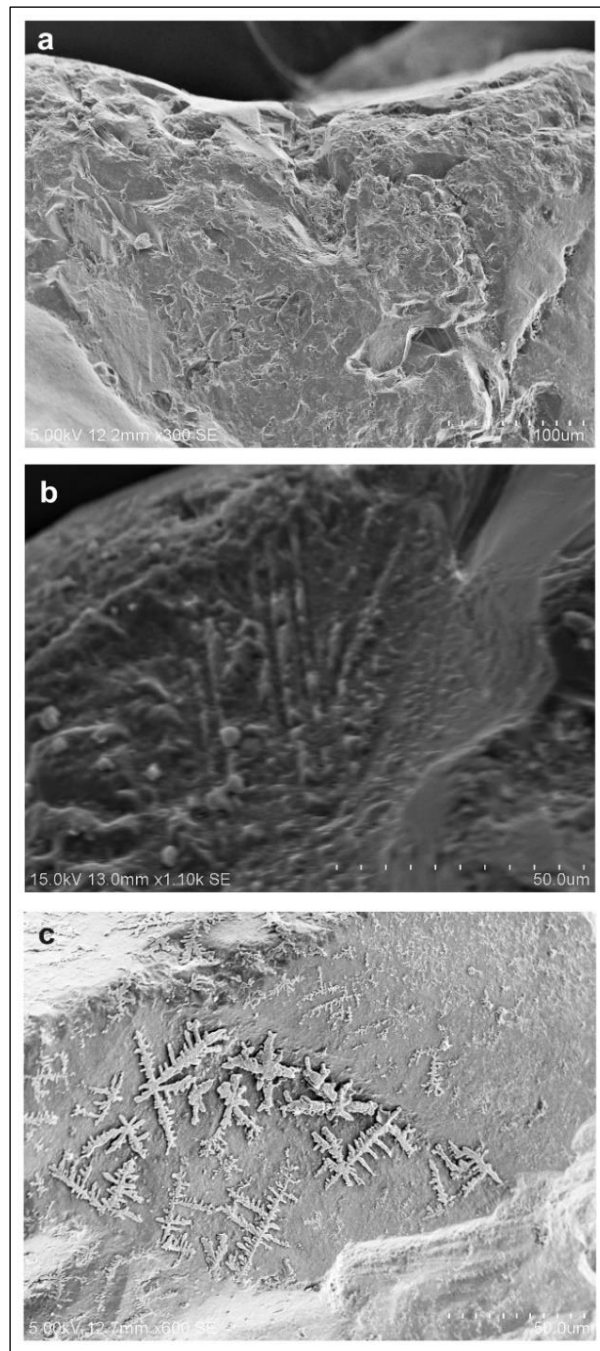


**Figure 4.8** SEM photomicrographs of representative quartz grains of fluvial miliolite samples from the KHF zone showing different types of silica precipitation. **a.** Uniform Si covering on an irregularly pitted and rough grain surface. **b.** Silica precipitation in the form of globules. **c.** Silica pellicle.

These are features resulting from the process of silica precipitation. These features represent various stages of silica precipitation. During the first stage of rapid silica precipitation globules are formed (Figure 4.8b). Such globules in the later stage merge to form silica flowers. Silica flowers further evolve into a silica pellicle (Figure 4.8c). Silica pellicles can cover the entire grain surface, which can sometimes obliterate other microtextures (Vos et al., 2014). The silica precipitation on the grain surface indicates that it has experienced diagenesis.

### **Aeolian microtextures**

Majority of the quartz grains (Figure 4.9) had a rounded to sub-rounded shape, which is a characteristic property of aeolian deposits. A grain with sharp edges exposing fresh fracture surface on its upper left portion and chemically weathered and rough surface can be seen (Figure 4.9a). A freshly exposed fracture surface on the upper edge of another grain (Figure 4.9b) and presence of depressions smoothed by solution action on most part of the grain surface can also be seen. Also, the edges of this grain are abraded and adhering particles can be noticed all over the grain surface. A fractured grain with rough surface and silica precipitation in the small grooves on the surface shows a crack progressing from the lower edge of the grain (Figure 4.9c). The next grain shows a set of linear fractures (Figure 4.9d) with a comparatively smooth surface having small conchoidal fractures and adhering particles. Small and large conchoidal fractures are visible with numerous irregular depressions all over one of the grain surfaces with large breakage blocks (Figure 4.9e). Sub-angular and highly fractured nature of grains can also be seen (Figure 4.9e, f). Here, the grain shows a rough surface with the presence of irregularly broken surfaces and upturned plates. The grains (Figure 4.9a, d and e) show bulbous edges as defined by Mahaney (2002) as prominent, protruding and rounded grain edges in the shape of a parabolic curve. The rounding of the edges and protrusions is attributed to the rotation of saltating grains, making this microtexture uncommon for grains smaller than 150  $\mu\text{m}$  (Mahaney, 2002). Therefore, the occurrence of bulbous edges is a diagnostic for aeolian transportation phases.

The broken and grooved surfaces result from severe grain-to-grain collisions during transport (Campbell, 1963). Figure 4.9f shows that the breakage of the grain has occurred perpendicular to each other which may be along plane of atomic weakness. It also shows straight and curved grooves on the surface with irregular depressions and abraded edges on the grain.

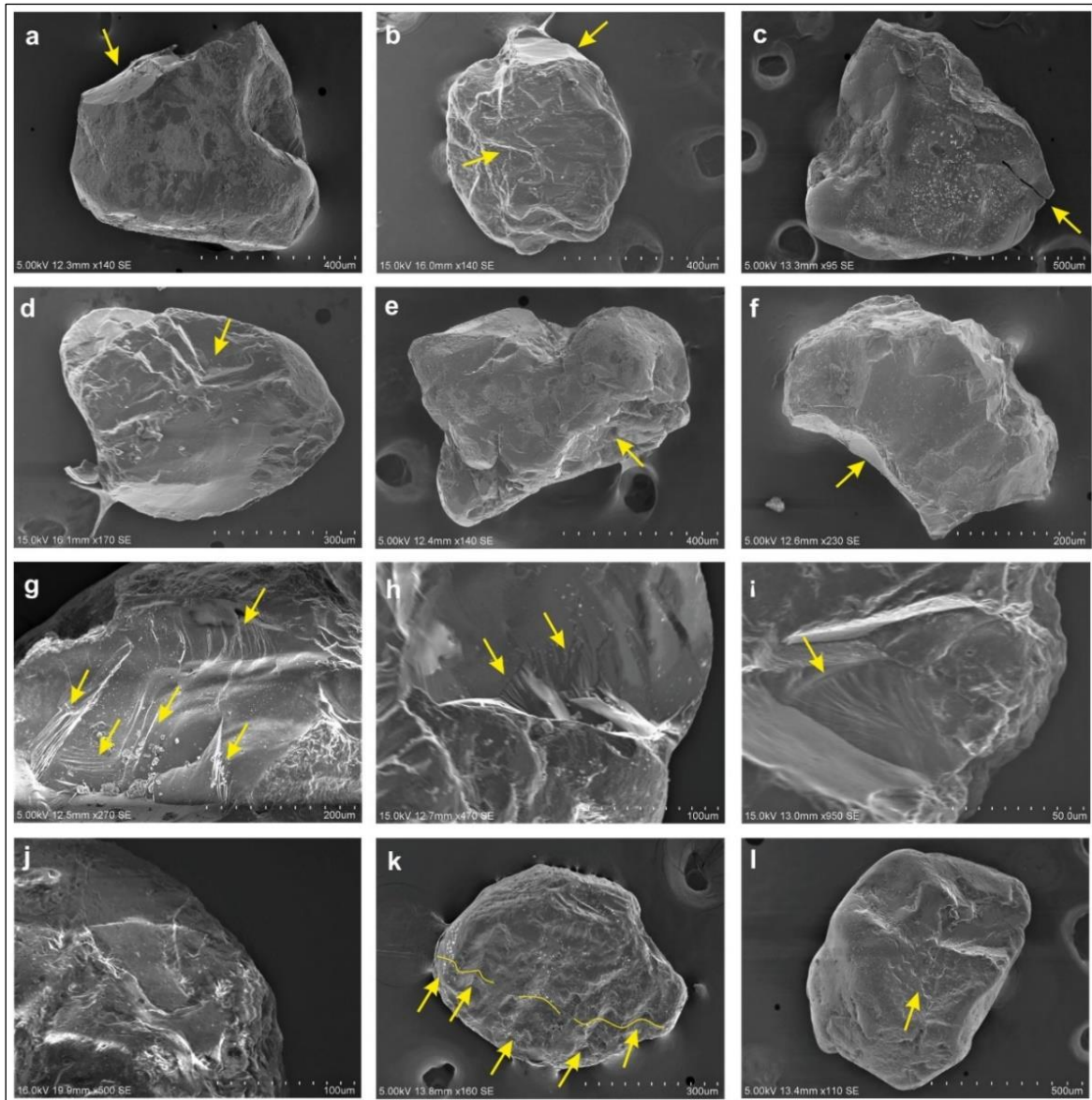


**Figure 4.9** SEM photomicrographs of representative quartz grains of aeolian miliolite samples from the KHF zone. **a.** Grain with sharp edges and chemically weathered and rough surface with fresh fracture surface on its upper left portion. **b.** Fractures and depressions on the surface smoothed by solution activity and fresh fracture surface on the upper edge of the grain. **c.** Intensively fractured grain with rough surface and silica precipitation in the small grooves and a crack propagating from the lower edge of the grain. **d.** Linear set of sub-parallel fractures developed with a comparatively smooth surface and small conchoidal fractures. **e.** Small and large conchoidal fractures with numerous irregular depressions all over the grain surface with large breakage blocks. **f.** Rough surface with the presence of irregularly broken surfaces and upturned plates. Note the sub-rounded and bulbous edges of the grains. **g.** Straight and parallel fractures oriented perpendicular to curved fractures (lower left corner) and exposed quartz cleavage plates in the lower right portion. **h.** and **i.** Radial fractures on the fresh fractured surface. **j.** Numerous unoriented, irregularly shaped pits and etched surface resulting due to solution action on the grain surface. **k.** Alternating crest and trough pattern made of few linear and almost parallel ridges formed on the grain surface. **l.** Grain surface displaying numerous v-shaped and crescentic percussion marks, abrasion marks, silica precipitation and adhering particles.

Most of the grains from the sample of aeolian miliolite showed the micro-feature of straight or parallel fractures (Figure 4.9g), which sometimes also occur in a curved manner, approaching the conchoidal fracture pattern. Figure 4.9h and i show a radial fracture pattern observed on the fresh fractured surface. Figure 4.9j shows the effect of solution on the grain surface by producing etched surface and irregular solution pits. The upper right portion of the grain can be seen slightly smoothed by solution action on a fresh fractured surface. Very eroded surface of the grain can be observed in Figure 4.9k. Remnants of conchoidal fractures can be seen on the upper portion of the grain, which is smoothed by solution action and silica precipitation.

More than half of the lower grain surface (Figure 4.9k) comprises of almost linear and parallel ridges displaying crest and trough pattern, given rise by collision between the grains during their transport (Campbell, 1963). The centre of the grain surface in Figure 4.9l shows numerous v-shaped and crescentic percussion marks, abrasion marks, silica precipitation and adhering particles. The presence of percussion marks indicated tough collision of the grains due to the high velocities of the winds transporting these sediments (Costa et al., 2013). Microtextures such as bulbous edges, straight and curved fractures, radial fractures are the most frequent features identified for the aeolian miliolite samples.